論文 89-26-6-6

An Analytical DC Model for HEMT's

(헴트 소자의 해석적 직류 모델)

金 榮 民*

(Young Min Kim)

要 約

헴트(HEMT)소자의 순수 해석적 DC모델이 2차원 전하제어 시뮬레이션 결과[4]에 기초하여 제작되었다. 이 모델에서는 2-DEG 채널의 전자 운송 역학에 확산 효과를 추가하였다. 이 확산효과는 기존 1차원 DC모델에서 사용하는 전자 이동도 및 문턱전압을 증가시키는 효과를 가졌음을 보였다. 또한 2-DEG 농도분포함수를 piecewise 선형화하여 HEMT 소자의 subthreshold 특성의 해석적 모델을추가하였고, 따라서 2-DEG의 채널두께 및 게이트 용량을 게이트 전압의 함수로 나타내었다. I-V curve의 전류포화영역에서의 기울기를 모델하는데는 gate 밑의 전자포화채널 지역에서의 전자채널두께와 채널길이 변조현상을 함께 고려하였다. Troffimenkoff형의 전장의존 전자이동도를 사용하여 I-V 곡선의 포화현상을 모델하였다. 또한 기존 1차원 모델에서 감안되지 않은 2차원 효과가 실제 전류특성곡선에서 매우 중요한 역할을 하며, 이 효과가 효과적으로 1개의 보정상수f로 보상됨을 보였고, 물리적으로 이 상수가 채널 GCA 지역과 채널포화지역 사이에 형성되는 채널천이지역의 전자농도와 관계됨을 보였다.

Abstract

A purely analytical model for HEMT's based on a two dimensional charge control simulation[4] is proposed. In this model proper treatment of diffusion effect of electron transport along a 2-DEG (two dimensional electron gas) channel is performed. This diffusion effect is shown to effectively increase the bulk mobility and threshold voltage of the I-V curves compared to the existing models. The channel thickness and gate capacitance are expressed as functions of gate voltages covering subthreshold characteristics of HEMT's analytically. By introducing the finite channel opening and an effective channel-length modulation, the slope of the saturation region of the I-V curves was modeled. The smooth transition of the I-V curves at linear-to-saturation regions of the I-V curves was possible using the continuous Troffimenkoff-type of field dependent mobility.

Furthermore, a correction factor f was introduced to account for the finite transition section forming between a GCA and a saturated section. This factor removes large discrepancies in the saturation region of the I-V curve predicted by existing 1-dimensional models.

*正會員, 韓國電子通信研究所 通信素子開發室
(Telecommunications Device Section, ETRI)

接受日字 : 1989年 4月 3日

I. Introduction

There has been continuing efforts on improving

HEMT's in recent years and as a consequence significant improvements have been made on both device fabrication and device models. With inherent superiority in speed and transconducatance to the GaAs MESFET devices, HEMT's have been showing promise for the future generation of switching elements. Recently 4K SRAM that demonstrated an access time of 2ns at 77°K[1] was introduced.

Stimulated by this progress in device fabrication, there have been several device models pubilshed. Some of two-dimensional numerical models concentrated on providing analyses on the electron transport characteristics along the 2-DEG channel formed in the AlGaAs/GaAs heterojunction[6], [8], [9]. The velocity-field relationship for the 2-DEG obtained from the Monte Carlo simulation suggests that mobility degradation mechanism at low electric field gives Si-like behavior and in contrast, after critical electric field, electron velocity saturates as in GaAs bulk.

Starting from a DC model that generates discontinuous I-V curves[10], A series of 1-dimensional models for HEMT's had been produced [11], [3], [5], [7]. However, due to inherent nonlinearity both in the charge control mechanism and the drain-voltage to drain-current characteristics, piecewise approximations have been made for the analysis of the device physics and resulted in discontiuous I-V curves or partly numerical models.

In this paper an analytical approach to the subthreshold characteristics is performed, which will allow us to model the gate capacitance as a function of gate voltage. Also the incorporation of diffusion current component is performed to account for the enhanced low-field mobility of the 2-DEG electrons compared to that of bulk electrons. The existence of the transition region between the GCA (Gradual Channel Approximation) section and saturated section is shown to be present by comparisons of measured data and existing two-section models. The transition section can be absorbed into the GCA section by incorporating a parameter f into the channel charge expression, which allows us to take advantage of using a simpler two-section model. This parameter turns out to be largely independent of both the gate voltages and drain voltages. This way we can have completely closed form of the I-V characteristics in both triode region and saturation region.

II. Nonlinear Piecewise Charge Control and 2-DEG Channel Thickness

Using the charge-sheet model[14] for channel electrons, the channel current can be written as

$$I = z\mu n_s \frac{dE_F}{dx} \tag{1}$$

where E_F represents a quasi Fermi level, μ the field-dependent mobility and n_s the concentration of the channel electrons. Denoting chemical potential as E_{Fi}, diffusion current component can be isolated from the quasi-Fermi level as

$$E_F = E_{Fi} - qV_c \tag{2}$$

On the other hand, the channel current can be written as

$$I = qz\mu n_s \varepsilon - qzD\frac{dn_s}{dx} \tag{3}$$

where parallel electric field ϵ and diffusion constant D are defined respectively as

$$\varepsilon = \frac{dV_c}{dx} \tag{4}$$

and

$$\frac{D}{\mu} = \frac{n_s}{q}\frac{dE_{Fi}}{dn_s} \tag{5}$$

The channel thickness is strongly dependent on the channel charge because the potential well confining the channel charge is mainly formed by the electric field from this charge itself. Here we are neglecting the background bulk charge, which is reasonable assumption especially for HEMT's having unintentional acceptor doping level of only 10^{14} cm^{-3}. The exact dependence of the channel thickness on applied gate voltages can be obtained from the 2-level 2-DEG concentration formula given in[4]. When there is no current flowing along the channel, the surface charge can be expressed using Lee's notation[3] as

$$n_s = \frac{K_0\varepsilon_0}{qd}\left(V_G - V_{th} - \frac{E_{Fi}}{q}\right) \tag{6}$$

where V_{th} represents a threshold voltage that can be expressed as

$$V_{th} = \phi_b - V_{P2} - \frac{\Delta E_c}{q} \tag{7}$$

where ϕ_b is the Shottkey barrier potential between AlGaAs and Al, $\triangle E_c$ the conduction band discontinuity and $V_{p2} = q N_d d_d^2/2\epsilon$.

Differentiation of Eq. 6 with respect to V_G results in

$$\frac{\partial n_s}{\partial V_G} = \frac{K_0 \varepsilon_0}{qd}\left(1 - \frac{1}{q}\frac{\partial n_s}{\partial V_G}\frac{dE_{Fi}}{dn_s}\right) \tag{8}$$

or

$$\frac{\partial n_s}{\partial V_G} = \frac{K_0 \varepsilon_0}{q\left(d + \frac{K_0 \varepsilon_0}{q^2}\frac{dE_{Fi}}{dn_s}\right)} \tag{9}$$

Then the gate capacitance can be expressed as

$$C_g \equiv q\frac{\partial n_s}{\partial V_G} = \frac{K_0 \varepsilon_0}{d + d_c} \tag{10}$$

where

$$d_c = \frac{K_0 \varepsilon_0}{q^2}\frac{dE_{Fi}}{dn_s} \tag{11}$$

and $d = d_d + d_i$. Eq. 11 is a general expression for the channel thickness which reflects the dependence of chemical potential upon the channel charge. Using Eq. 10, n_s can be written as follows since $V_G - V_{th}$ can be regarded as the voltage difference between the gate and the channel charge,

$$n_s = \frac{K_0 \varepsilon_0}{q(d + d_c)}(V_G - V_{th}) \tag{12}$$

In general, d_c can be evaluated as a function of V_G using Eq. 11 and Eq. 12 by iteration utilizing the fact that dE_{Fi}/dn_s is a function of n_s only (the functional dependence of E_{Fi} upon n_s is in[6]). However, for CAD purposes this approach is not appropriate. Eq. 5 can be drawn using the E_{Fi} vs n_s curves published elsewhere and shown in Fig. 1. As can be seen from the relation between D/μ and n_s in this figure, we can approximate this curve with two pieces, i.e., one as a linear curve and the other as a parabolic curve. In the linear region where n_s is large

$$\frac{D}{\mu} \equiv \frac{1}{q} n_s \frac{dE_{Fi}}{dn_s} = b' + a' n_s \tag{13}$$

where

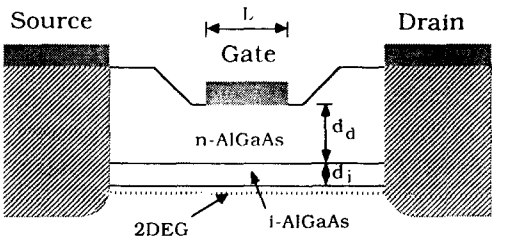

Fig.1. Structure of typical HEMT.

$b' = 0.0305$ (V)

$a' = 1.5 \times 10^{-17}$ (V m²)

and for the parabolic region where n_s is small

$$\frac{D}{\mu} \equiv \frac{1}{q} n_s \frac{dE_{Fi}}{dn_s} = 0.0259 + \sqrt{a_i' n_s} \tag{14}$$

where $a' = 3.2 \times 10^{-19}$ ($V^2 m^{-2}$). The splitting point between these two regions was chosen so as to have the best reproduction of the original curve, which turns out to be $n_s = 3.8 \times 10^{14}$ m^{-2}. For the linear region, from Eq. 11

$$d_c = \frac{K_0 \varepsilon_0}{q^2}\frac{dE_{Fi}}{dn_s} = \frac{b}{n_s} + a \tag{15}$$

where

$$a = \frac{K_0 \varepsilon_0}{q} a'$$

$$b = \frac{K_0 \varepsilon_0}{q} b'$$

Then d_c can be evaluated combining Eq. 12 and Eq. 15 as

$$d_c = \frac{(a+d)b}{(K_0 \varepsilon_0/q)(V_G - V_{th}) - b} + a \tag{16}$$

The gate capacitance associated with the channel thickness for the linear region can be obtained from Eq. 10 and Eq. 16 as

$$C_g = \frac{K_0 \varepsilon_0/q (V_G - V_{th}) - b}{(a+d)(V_G - V_{th})} \tag{17}$$

For the parabolic region, from Eq. 14

$$d_c = \frac{K_0\varepsilon_0}{q^2}\frac{dE_{F1}}{dn_s} = \frac{\sqrt{a_1}}{\sqrt{n_s}} + \frac{c_1}{n_s} \tag{18}$$

where

$$\sqrt{a_1} = \frac{K_0\varepsilon_0}{q}\sqrt{a_1'}$$

$$c_1 = 0.025\frac{K_0\varepsilon_0}{q}$$

Then d_C can be evaluated from Eq. 12 and 18 as

$$C_g = \frac{q\left[-\frac{\sqrt{a_1}}{2d} + \sqrt{\frac{a_1}{4d^2} + \frac{K_0\varepsilon_0}{qd}(V_G - V_{th}) - \frac{c_1}{d}}\right]^2}{K_0\varepsilon_0(V_G - V_{th})} \tag{19}$$

The gate capacitance associated with this channel opening can be obtained from Eq. 10 and Eq. 19 as

$$d_c = \frac{K_0\varepsilon_0(V_G - V_{th})}{q\left[-\frac{\sqrt{a_1}}{2d} + \sqrt{\frac{a_1}{4d^2} + \frac{K_0\varepsilon_0}{qd}(V_G - V_{th}) - \frac{c_1}{d}}\right]^2} - d \tag{20}$$

Fig.2 and 10 shows the plot for the gate capacitance and the channel thickness as functions of gate voltages respectively. We can observe that the channel thickness is almost constant near the value of around 100 A when the gate voltage is well above the threshold voltage which is 0.25 V for this particular example. As the gate voltage approaches to the threshold voltage, the gate capacitance is decreasing due to the charge spreading into the bulk GaAs.

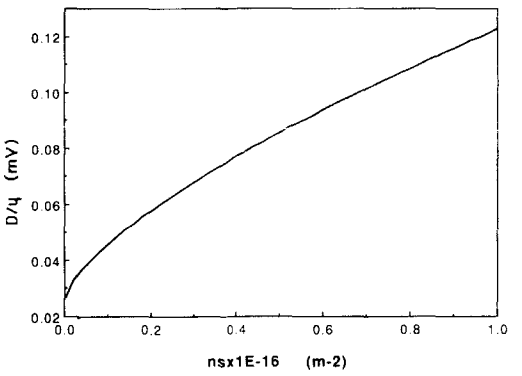

Fig.2. D/μ vs n_s at room temperature.

On the other hand, the electron concentration in the GCA section can be represented by the charge control equation

$$n_s = \frac{C_g}{q}(V_{off} - V_C) \tag{21}$$

where

$$V_{off} = V_G - V_{th} \tag{22}$$

Differentiation of Eq. 21 with respect to x leads to

$$\frac{dn_s}{dx} = -\frac{C_g\varepsilon}{q} \tag{23}$$

Combining Eqs. 3, 13, 21 and 23

$$I = z\mu'\varepsilon C_g(V'_{off} - V_C)$$

$$= z\left(\frac{C_g a'}{q} + 1\right)vC_g(V'_{off} - V_C) \tag{24}$$

where

$$\mu' = \mu\left(\frac{C_g a'}{q} + 1\right) = \frac{\mu_0\varepsilon}{1 + \varepsilon/\varepsilon_c}\left(\frac{C_g a'}{q} + 1\right) \tag{25}$$

and

$$V'_{off} = V_{off} + \frac{b'}{C_g a'/q + 1} \tag{26}$$

From Eqs. 25 and 26, we can conclude that the increase of total current by the 2-DEG diffusion effect is equivalent to an increase of the low-field mobility and also to an increase of the threshold voltage comparing the low-field mobility and the threshold voltage that are defined as the values for the case when the diffusion current component has been neglected. This phenomenon may explain one of the reasons for the enhanced low-field mobility of 2-DEG compared to that of the 3-DEG usually observed for the quantum well devices. If we consider the Troffimenkoff type of field-dependent mobility with $\beta = 1$, electron velocity

$$v = \mu\varepsilon = \frac{\mu_0\varepsilon}{1 + \varepsilon/\varepsilon_c}; \quad \varepsilon \leq \varepsilon_p \tag{27}$$

where μ_0 denotes the low-field mobility and ϵ_c the critical electric field where full velocity saturation of electron occurs.

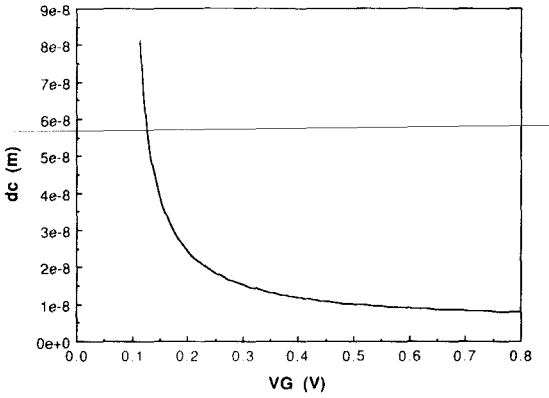

Fig.3. Channel thickness vs gate voltage.

III. I-V Curves for Triode Region

As pointed out in the previous section, there exists a transition section between the GCA and saturated section, where neither normal electric field nor parallel electric field component could be neglected in the 2-dimensional Poisson's equation. Fig. 4 shows the boundary conditions along the channel including the transition section.

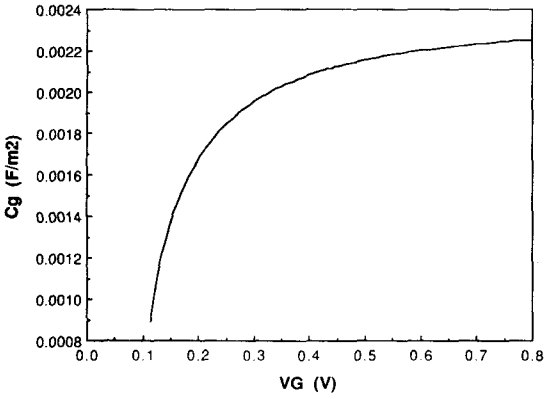

Fig.4. Gate capacitance vs gate voltage.

On the other hand, the Poisson's equation in the GaAs region neglecting GaAs bulk acceptor concentration is

$$\frac{\partial^2 V}{\partial y^2}+\frac{\partial^2 V}{\partial x^2}=\frac{q}{K_s\epsilon_0}n \tag{28}$$

where n represents the 3-dimensional electron gas concentration. Integrating Eq. 28 along y direction (y direction corresponds to that normal to heterointerface with y=0 corresponding to the location of heterointerface)

$$\int_{-\infty}^{0}\frac{\partial^2 V}{\partial y^2}dy^2+\int_{-\infty}^{0}\frac{\partial^2 V}{\partial x^2}dy=\frac{q}{K_s\epsilon_0}\int_{-\infty}^{0}ndy \tag{29}$$

which reduces to

$$\epsilon+d_c\frac{d^2V_c}{dx^2}=\frac{q}{K_s\epsilon_0}n_s \tag{30}$$

where d_c represents the effective channel thickness for zero drain voltage in the GCA section. If a GCA expression is used for ϵ_{normal}

$$n_s=C_g(V'_{off}-V_c)+K_s\epsilon_0 d_c\frac{d^2V_c}{dx^2} \tag{31}$$

The second term of this equation represents the electron concentration coupled with the parallel electric field, which is free from the control of the gate voltage. This term is assumed to be proportional to the channel potential V_c based on the 2-dimentional analysis of the channel potential at the drain side of the potential barrier, where the channel potential V_c is shown to vary as the hyperbolic sine function of x.

$$K_s\epsilon_0 d_c\frac{d^2V_c}{dx^2}=fC_gV_c \tag{32}$$

where f denotes the proportionality constant. From Eq. 32, we can easily notice that V_c has hyperbolic sine dependence on x the channel direction. Then combining Eqs. 31 and 32, the total electron concentration n_s is

$$n_s=\frac{C'_g}{q}(V''_{off}-V_c) \tag{33}$$

where

$$C_g' = C_g(1-f)$$

and

$$V_{of}'' = \frac{V_{off}'}{1-f}$$

The 2nd term of Eq. 31 is associated with the parallel component of the electric field along the channel and cannot be neglected in the transition section from GCA to saturated section even though the 1st term can be neglected in the saturated section and 2nd term can be neglected in the GCA section. Eq. 33 tells us that transition section can be absorbed as part of the GCA section by using the reduced capacitance C_g' and increased pinch-off voltage V_{off}''. This fact implies that transition section can be extended to the GCA section with reduced total charge control capacitance C_g'. Also the increased V_{off}'' enforces electron pinching off to be delayed for the applied drain voltage due to the increase of electrons accumulated by the parallel electric field in the saturated section. Then, these modified charge control parameters can be used in the existing two-section model to generate more accurate results. Then Eq. 24 becomes

$$I_D = \beta \frac{\varepsilon}{1+\varepsilon/\varepsilon_C}(V_{off}'' - V_C) \tag{34}$$

where

$$\beta = z\mu_0\left(1 + \frac{C_g a'}{q}\right)C_g' \tag{35}$$

Solving Eq. 34 for ϵ

$$I_D = \left[\beta(V_{off}'' - V_C) - \frac{I_D}{\varepsilon_C}\right]\varepsilon \tag{36}$$

Integrating Eq. 36 from x =0 to x =L

$$I_D = \frac{\beta}{L + V_D/\varepsilon_C}\left(V_{off}'' V_D - \frac{1}{2}V_D^2\right) \tag{37}$$

IV. I-V Curves for Saturation Region

Based on the properties of HEMT's previously discussed, a two-section model which is shown in Fig. 4, can be established. This figure corresponds to the case when applied drain voltage is well above the saturation voltage. In this fugure, d_c and d_s represents the channel thickness of the GCA section and the saturated section respectively The electron velocity at the saturated section can be asumed to be in full saturation without appreciable error. When the operating point is in the saturation region of the I-V curves, a saturated section is already formed in the drain side of the channel and in this case Fig.4 can be used for the boundary conditions along the channel. Now if we define $x_p = 0$ or $x = L'$ to be the splitting point between the GCA and the saturated section with ϵ_p and $V_c(L')$ being the parallel electric field and the channel voltage at that point respectively, the saturation current can be written as follows. From Eq. 37 assuming $V_c(L') = V_p$

$$I_D = \frac{\beta}{L' + V_P/\varepsilon_C}\left(V_{off}'' V_P - \frac{1}{2}V_P^2\right) \tag{38}$$

This equation tells us that as the drain voltage increases beyond the saturation voltage, L' becomes smaller than L and accordingly the current will increase. This current increase beyond saturation essentially implies a finite slop in the saturation region of the I-V curves. Then V_p can be calculated from the linear region of the I-V curves. From Eq. 37

$$I_P = \frac{\beta}{L + V_P/\varepsilon_C}\left(V_{off}'' V_P - \frac{1}{2}V_P^2\right) \tag{39}$$

Also from Eq. 34

$$I_P = \beta \frac{\varepsilon_P}{1+\varepsilon_P/\varepsilon_C}(V_{off}'' - V_P) \tag{40}$$

Elimination of I from Eqs. 39 and 40 and solving for V_p results in

$$V_P = -\frac{\varepsilon_C(V_{off}'' + \varepsilon_P L)}{\varepsilon_P - \varepsilon_C} + \sqrt{\left(\frac{\varepsilon_C(V_{off}'' + \varepsilon_P L)}{\varepsilon_P - \varepsilon_C}\right)^2 + \frac{2\varepsilon_C\varepsilon_P L V_{off}''}{\varepsilon_P - \varepsilon_C}} \tag{41}$$

Then I_p can be obtained from Eqs. 40 and 41. On the other hand, at the pinch-off point of the I-V curves, the saturated section just start forming at the drain side edge. As the I-V curves moves into the saturation region, the velocity

saturated section moves into the channel under the gate. The charge in the saturated section is velocity saturated due to the high parallel electric field and therefore charge coupled with normal electric field (gate controled charge) is negligible compared to the charge controlled by the parallel electric field. Therefore the first term in Eq. 31 is discarded and channel thickness d_s is used instead of d_c the channel thickness for the GCA section. In general channel thickness in the saturation region should be much larger than that of GCA section due to the lack of the normal electric field or the 2-DEG density as can observed from Fig. 2 since we know that the gate voltage is directly related with the normal electric field.

From Eq. 3 the drain current in the saturated section neglecting diffusion term

$$I_D = qz\left(1 + \frac{C_g a'}{q}\right) n_s v \tag{42}$$

And by using full velocity saturatin in the saturated section, i.e., $V=V_s$, and neglecting the normal component of n_s in Eq. 31 where $d_c = d_s$, then Eq. 42 can be written as

$$\frac{d^2 V_c}{dx^2} = \frac{I_D}{K_s \varepsilon_0 d_s z\,(1 + C_g a'/q)\, v_s} \tag{43}$$

Integrating Eq. 43 twice with respect to x from x = L′ to L or $x_p=0$ to $\triangle L$ and $V_c=V_p$ to V_D (refer to Fig.4), we obtain

$$V_D - V_P = K I_D (\Delta L)^2 + \varepsilon_P \Delta L \tag{44}$$

where

$$K = \frac{1}{2K_s \varepsilon_0 d_s z\,(1 + C_g a'/q)\, v_s} \tag{45}$$

Here in the integrating process, continuity of electric field at the boundary of transition section and saturated section ($\epsilon=\epsilon_p$ at x = L′) was imposed. Using L=L′ + $\triangle$L, Eq. 38 reduces to

$$I_D \Delta L = (L + V_P/\varepsilon_C)\,(I_D - I_P) \tag{46}$$

Multiplying Eq. 44 by I_D and combining it with Eq. 46 to eliminate the term involving $I_D \triangle L$,

$$I_D (V_D - V_P) = K (L + V_P/\varepsilon_C)^2 (I_D - I_P)^2 + \varepsilon_P (L + V_P/\varepsilon_C)\,(I_D - I_P) \tag{47}$$

From Eq. 47, it can be easily verified that if $V_D=V_p$, then $I_D=I_p$ or vice versa. This result ensures the continuity of the linear region and the saturation region of the I-V curves at that point. Solving Eq. 47 for (I_D-I_p)

$$I_D = I_P - \frac{\varepsilon_P (L + V_P/\varepsilon_C) - (V_D - V_P)}{2K (L + V_P/\varepsilon_C)^2} + \sqrt{\left(\frac{\varepsilon_P (L + V_P/\varepsilon_C) - (V_D - V_P)}{2K (L + V_P/\varepsilon_C)^2}\right)^2 + \frac{(V_D - V_P) I_P}{K (L + V_P/\varepsilon_C)^2}} \tag{48}$$

Eq. 48 describes the I_D versus V_D relationship purely analytically in the saturation region of the I-V curves. Once V_p and I_p are calculated from Eqs. 41 and 40, one can generate I-V curves of the saturation region easily using Eq. 48. Therefore, Eqs. 37 and 48 constitute complete equations for the I-V curves in the whole operational range for HEMT's DC behavior.

V. I-V Curves

Fig.5 shows a comparison between the two section model without f factor and the experimental data[3]. The solid line corresponds to the measured data and the dotted line corresponds to the present model. In this comparison , we can see that in the linear region of the I-V curves, good agreement is achieved. However, as the saturation region is reached, there are huge differences in the saturation current levels. Most of the 1-dimensional models published which incorporated Troffimenkoff type of field-dependent mobility use decreased threshold voltage to align the saturation regions of the I-V curves. However, this method creates a discrepancy in the linear region of the I-V curves. In order to eliminate this discrepancy, they had to again increase the source resistance values to obtain a reasonable fit for the entire range of I-V curves. The source resistance usually used were almost two times as large as the measured value[7],[11]. This approach is inadequate because it may not be a good approach to use the source resistance and threshold voltage

as fitting parameters. When the f factor was introduced in the current *two-section model*, we could observe excellent agreement with the experimental data as can be seen in Fig.6. Table 1 lists the device parameters used in Fig.5 and Fig.6. Actually the I-V fittings without af factor cannot avoid the considerable discrepancies near the knee regions of the I-V curves even though overall fittings are reasonable.

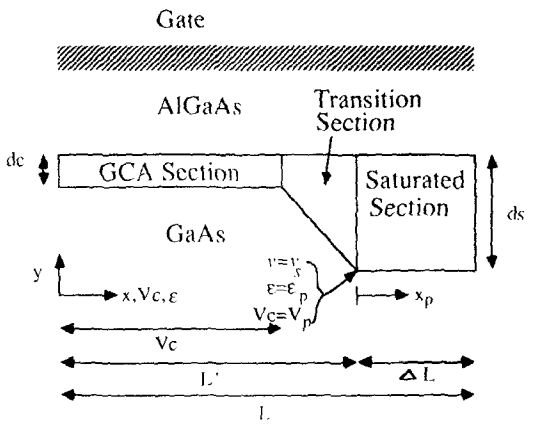

Fig.5. Boundary condition for two-section model.

Tabel 1. Device parameters for I-V comparision for Fig. 6 and Fig. 7.

Device Parameter	Experimental Data	Model Parameter
μ_0 (cm^0 (cm^2/V_s	4300	1600
v_s (m/s))	-	1×10^5
d_a (A)	300	300
d_i (A)	300	100
N_D (cm^{-3})	1×10^{18}	1×10^{18}
ΔE_c (eV)	-	0.32
ϕ_m (eV)	-	1.05
z (μ)	145	145
L (μ)	1	1
R_s (Ω)	12	12
f	-	0.2
d_s (A)	-	300

Fig. 7 and 8 shows another example of the I-V comparisons between experimental data[12] and the 2-section model with and without the f factor respectively. Table 2. lists the device parameters associated with this comparison. Again we observe the same phenomenon as the previous comparison except that a slightly different value of f was involved. In the linear region of the I-V curves, we observe absolute agreement. However, the 2-section model without f factor underestimates the saturation currents. Through repetitive I-V fitting process, it has been

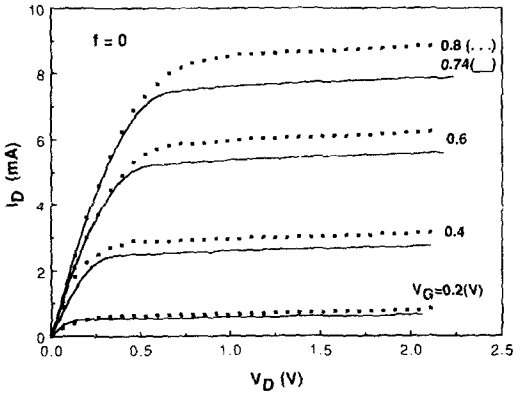

Fig.6. Comparison of I-V curves. Solid line: two-section model with correction factor f=0, dotted line: experimental data.

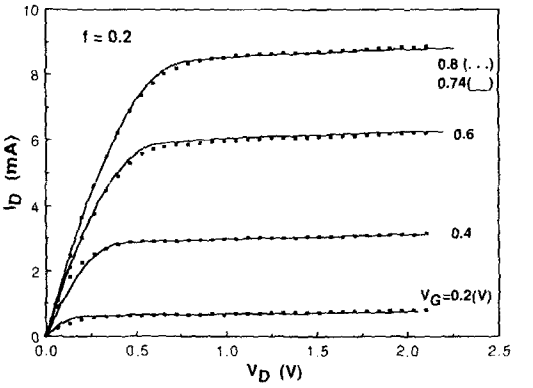

Fig.7. Comparison of I-V curves. solid line: two-section model with correction factor f=0.2, dotted line: experimental data.

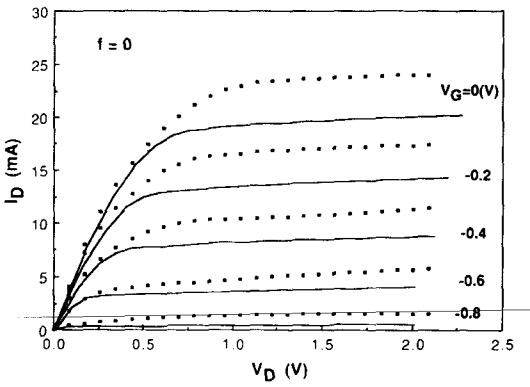

Fig.8. Comparison of I-V curves. solid line: two-section model with correction factor f=0, dotted line: experimental data.

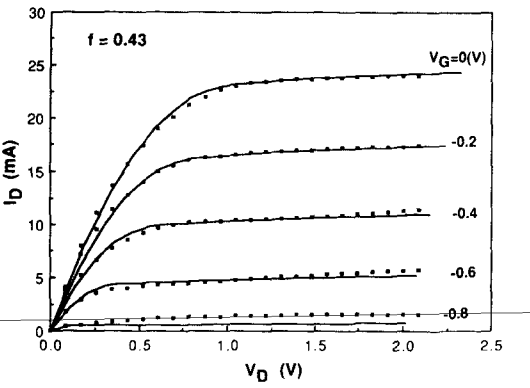

Fig.9. Comparison of I-V curves. solid line: two-section model with correction factor f= 0.2, dotted line: experimental data.

Table 2. Device parameters for I-V comparision for Fig. 8 and Fig. 9.

Device Parameter	Experimental Data	Model Parameter
μ_0 (cm^2/V_s)	4300	4500
v_s (m/s)	–	1.75×10^5
d_d (A)	350	450
d_i (A)	60	60
N_D (cm^{-3})	1×10^{18}	1×10^{18}
ΔE_c (eV)	–	0.32
ϕ_m (eV)	–	1.05
z (μ)	145	145
L (μ)	1	1
R_s (Ω)	7	7
f	–	0.43
d_s (A)	–	1000

found that the agreement for the whole range of I-V curves can only be achieved by introducing the f factor. During the I-V simulation process, it was found out that the slopes of the saturation region of the I-V curves are largely dependent on d_s the thickness of the channel in the saturated section and ϵ_p the parallel electric field at the boundary between the transition section and the saturated section.

IV. Conclusion

A compleletely analytical model for HEMT's was discussed. Diffusion effects, nonlinear charge control, and f factor explaining the 2-dimensional effects are effectively modeled to give good fit to the measured I-V curves. This model will give great advantages in integrating it into a circuit simulator programs such as SPICE. Also, analytical circuit parameters c d be easily extracted from this model for large AC signal analysis for HEMT's circuits and will be published in near future.

References

[1] S. Kurota et al., "New device structure for 4Kb HEMT SRAM," *in Tech. Dig., IEEE Gallium Arsenide Integrated Circuit Symp.* (Boston, MA), Oct. 1984.

[2] D. Delagebeaudeuf and N.T. Linh, "Metal-(n) AlgaAs-GaAs two-dimensional electron gas FET," *IEEE Trans. Electron Devices*, vol. ED-29, pp. 955-960, June 1982.

[3] T.J. Drummond, H. Morkoc, K. Lee, and M. Shur, "Model for modulation-doped field effect transistor," *IEEE Electron Device Lett.*, EDL-3, pp. 338-341, Nov. 1982.

[4] Young Min Kim and P. Roblin, "Two-dimensional charge control model for MODFETs," *IEEE Trans. on Electron Devices*, vol. 22, Nov. 1986.

[5] K. Lee et al., "Current-voltage and capacitance-voltage characteristics of modulation-doped field-effect transistors," *IEEE Trans.*

Electron Devices, vol. ED-30, no. 3, March 1983.

[6] Young Min Kim, "A two-dimensional charge control model and an analytical CAD model for MODFET's," Ph. D. Dissertation, Electrical Engineering, Ohio State University, Dec. 1986.

[7] M.H. Weiler and Y. Ayasli, "DC and microwave models for AlGaAs/GaAs high electron mobility transistors," *IEEE Trans. Electron Devices*, vol. ED-31, p. 1854, 1984.

[8] M. Mouis et al., "Aspect ratio phenomena in the high electron mobility transistor," *Proceedings IEEE/Connel Conference on Advanced Concepts in High Speed Semiconductor Devices and Circuits*, p. 144, July 1985.

[9] J. Yoshida and M. Kurata, "Analysis of high electron mobility transistors based on a two-dimensional numerical model," *IEEE Electron Device Lett.*, vol. EDL-5, pp. 508, 1984.

[10] H. Rohdin and P. Roblin, "A MODFET dc model with improved pinchoff and saturation characteristics," *IEEE Trans. Electron Devices*, vol. ED-33, no. 5, May 1986.

[11] Kwangmean Park and Kae Dal Kwack," A model for the current-voltage characteristics of MODFET's," *IEEE Trans. Electron Devices*, vol. ED-33, no. 5, May 1986.

[12] H. Morkoc, "High speed modulation-doped AlGaAs/GaAs field effect transistors: MODFET's); analysis, fabrication and performance," Internal Reports, Department of Electrical Engineering and Coordinated Science Laboratory, University of Illinois.

[13] F.N. Troffimenkoff, *Proc. IEEE*, vol. 53., pp. 1765, 1965.

[14] J.R. Brews, "A charge-sheet model of the MOSFET," Solid State Electronics, vol. 21, pp. 345-355, 1978. *

著 者 紹 介

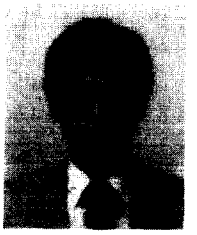

金 榮 民(正會員)

1954年 4月 18日生. 1976年 서울대학교 전자공학과 공학사학위 취득. 1978年 한국과학기술원 전기 및 전자공학과 공학석사학위 취득. 1982年～1986年 미국 OHIO STATE UNIVERSITY전기공학과 공학박사학위 취득. 1986年～1988年 미국 North Carolina A & T State University 전기과 교수. 현재 한국전자통신연구소 통신소자개발실 실장. 주관심 분야는 HEMT 소자 및 고속 고집적 통신소자, BiCMOS 등임.